We are IntechOpen, the world's leading publisher of Open Access books

Built by scientists, for scientists

4,800
Open access books available

122,000
International authors and editors

135M
Downloads

Our authors are among the

154
Countries delivered to

TOP 1%
most cited scientists

12.2%
Contributors from top 500 universities

WEB OF SCIENCE™

Selection of our books indexed in the Book Citation Index
in Web of Science™ Core Collection (BKCI)

Interested in publishing with us?
Contact book.department@intechopen.com

Chapter

Performance Evaluation and Control Strategy Comparison of Supercapacitors for a Hybrid Electric Vehicle

Enhua Wang, Minggao Ouyang, Fujun Zhang
and Changlu Zhao

Abstract

Electrification of powertrain system is a great technical progress of traditional vehicle, leading to a significant reduction of fuel consumption and emission pollution. Energy storage system (ESS) normally consisting of batteries is a key component of an electric vehicle or hybrid electric vehicle. An ESS can recover braking energy during the regenerative braking process. Currently, lithium-ion batteries are the main energy storage device due to their high energy density. However, sometimes, a sudden large increase of operation current is required during acceleration or regenerative braking processes, which will jeopardize the operation life of batteries. A supercapacitor takes advantage of high power density and can tolerate large current in a short time. Application of supercapacitor in an ESS can reduce the peak current of batteries effectively, and the life time of batteries can be extended. Meanwhile, the braking energy can also be recovered sufficiently. Supercapacitors can be used solely in some hybrid electric vehicles. In this chapter, the application of supercapacitors in electric vehicles or hybrid electric vehicles is reviewed briefly. Then, the performance of a series hybrid transit bus, which uses a compressed natural gas engine and supercapacitors as power sources, is analyzed.

Keywords: supercapacitors, transit bus, control strategy, dynamic programming, series hybrid

1. Introduction

A transit bus is a prime commuting tool for city residents, which consumes lots of fuel every year and produces a huge amount of poisonous emissions [1]. Electrification of transit bus is a good solution for these problems. Normally, the energy storage device consists of batteries [2]. The supercapacitor is a newly developed high-power electrochemical energy storage component [3, 4]. Farkas and Bonert have predicted that a supercapacitor is a good solution for hybrid vehicles [5]. Recently, many researches were performed to study the characteristics of supercapacitors as the energy storage system (ESS) of a hybrid electric vehicle (HEV) [6, 7].

Supercapacitors have a large surface area of electrode materials, which normally are activated carbons, and a very thin electrolytic separator leading to a very high capacitance. They store energy electrostatically. For automotive applications, most of them are electrochemical double-layer capacitors (EDLCs) [8]. Supercapacitors have a very high power density, which is over 10 times than batteries and can be charged or discharged up to 1,000,000 times which is significantly larger than lithium-ion batteries. They also have a very long life time and a wide operation temperature range [9].

Because supercapacitors have a high power density and can be charged or discharged in a short time, they can be used as a sole ESS for transit bus, which undergoes a frequent acceleration and deceleration processes. The first known transit bus powered by supercapacitors alone is Capabus operating in Shanghai since 2010. The buses were manufactured by Sunwin Bus Co., Ltd., and the supercapacitors were provided by Shanghai Aowei Co., Ltd. The transit bus can run 8–10 km each time after being fully charged. A total mileage of several million kilometers has been achieved, and the average energy consumption is close to 0.98 kWh/km [10]. Many other bus manufacturers also developed their products. Higer Bus Co., Ltd. together with an Israeli-Bulgarian bus company designed a transit bus with 20 kWh supercapacitors named as Chariot e-bus [10].

Supercapacitors have a low energy density of up to 10 Wh/kg. However, batteries especially lithium-ion batteries take advantage of high energy density which can be over 180 Wh/kg. For most automotive applications such as a plug-in hybrid electric vehicle (PHEV) or electric vehicle (EV), the ESS should guarantee a driving distance of more than 50 km normally, which can cover over 80% of people's daily travel in Beijing. Therefore, supercapacitors are combined together with batteries as a hybrid energy storage system (HESS). The batteries provide average energy, while the supercapacitors absorb energy during regenerative braking or discharge energy during acceleration. As a result, the high-rate working conditions of the batteries are avoided, and their life spans are extended. On the other hand, the internal resistance of a supercapacitor is much lower than that of a battery; the energy efficiency of a vehicle with an HESS is also improved compared with only batteries. Moreover, the size of the ESS can be decreased if supercapacitors are used. Accordingly, the cost can be reduced. There are mainly three kinds of topologies for HESS: passive, semi-active, and active [11]. Currently, supercapacitor semi-active topology shows a better performance considering efficiency, size, cost, and complexity [12]. Many studies were carried out to determine the size of HESS and optimize the energy management [13–16].

Control strategy design of a hybrid transit bus has important impact on system performance. The control strategy can be categorized as rule-based and optimization-based strategies [17, 18]. Rule-based control strategy specifies the power distribution between the auxiliary power unit (APU) and the ESS based on a set of rules according to the power demand of a vehicle and the state of charge (SOC) of ESS. Thermostatic control, power follower control, and fuzzy logic control are three types of rule-based control strategies [19–23]. Because these strategies do not need information of future driving conditions and have a low computation load, they are appropriate for real-time control application. Optimization-based control strategy splits the power demand based on an optimal algorithm and a mathematical model of the hybrid powertrain. They require the details of the entire driving profile. Normally, they are a kind of global optimization method such as dynamic programming [24], optimal control strategy [25–27], and neural network control [28]. Optimization-based control strategy can be used to estimate the theoretical maximum energy efficiency. However, it requires future information of the driving

velocity and has a huge computation load. Therefore, it is infeasible for a practical real-time vehicle system.

In this chapter, a series hybrid transit bus powered by a compressed natural gas (CNG) engine and supercapacitors is studied. The energy conversion characteristics of the designed series hybrid powertrain are analyzed using a mathematical model. First, two rule-based control strategies—the thermostatic control and the power follower control—are designed and compared. Later, the maximum potential of energy savings is estimated using an optimal control strategy based on dynamic programming. Finally, the operation characteristics of the series hybrid powertrain using the different control strategies are discussed. The results of this study provide a demonstration on how to design an ESS for an electric vehicle or hybrid electric vehicle from the systematic level.

2. System description

The designed series hybrid powertrain for a transit bus is described as follows. A CNG engine is directly connected with a permanent magnetic synchronous genera- tor (PMSG). A high-voltage power line is connected to the generator and the ESS as well as a permanent magnetic synchronous motor (PMSM). The PMSM connected to the final drive is a specially designed low-speed and high-power PMSM. The engine is a Yuchai 6.5 L CNG engine whose rated power is 140 kW. Both the PMSG and the PMSM are developed by Jing-Jin Electric Technologies (Beijing) Co., Ltd. The PMSG is a low-speed and high-efficiency electric machine whose rated power is 135 kW. The rated power of the PMSM is slightly greater than that of the PMSG. These two high-power electric machines have already been applied to several dif- ferent types of hybrid vehicles successfully. The ESS includes three parallel groups of supercapacitors, and each group consists of 13 units of Maxwell 48 V module connected in series. The total energy capacity of the ESS is 2.115 kWh, and the rated voltage is 624 V. To keep the supercapacitors from overdischarging, the minimum operation voltage of the ESS is set to 300 V.

The working principle of the designed series hybrid powertrain can be explained by an energy flow diagram shown in **Figure 1**. When the series hybrid transit bus is running, four different operation modes are defined according to the working conditions. Two modes are used for the driving conditions, and the other two modes are for the regenerative braking conditions. For the driving mode A, the
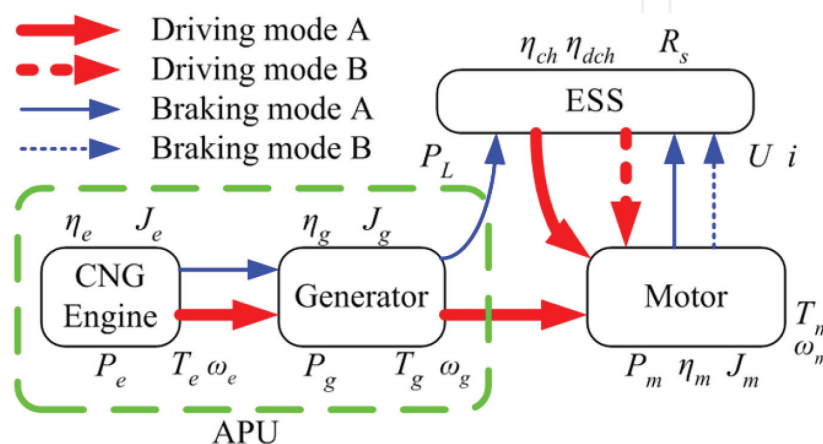
Figure 1.
Energy flow diagram of the series hybrid transit bus.

CNG engine is running, and the APU together with the ESS supplies electric power to the motor. This driving mode is activated if the required driving power is high or the SOC is low. When the SOC is high and the required driving power is less than a certain value, the ESS provides electric energy to the motor alone as the driving mode B shows. If the series hybrid bus is braking, the regenerative energy output from the motor is supplied to the ESS. Meanwhile, the APU can be activated or deactivated denoted by the braking modes A and B, respectively.

3. Mathematical model

A mathematical model is established according to the working principle of the designed series hybrid powertrain. The corresponding parameters of the hybrid transit bus are listed in **Table 1**. The tractive force acting on a rear-wheel-driven two-axle vehicle can be determined according to the corresponding longitudinal dynamic equation expressed as

$$F = mg \cos \alpha \left(f_1 + f_2 v \right) + \frac{1}{2} \rho A C_D v_r^2 + mg \sin \alpha + \delta m \frac{dv}{dt}. \tag{1}$$

The wheel and axle model first calculates the front axle load and the rear axle load according to the technical parameters of the series hybrid transit bus. Then, the tractive force coefficient of the rear tires can be determined. The slip of the tires can be modeled as a function of the tractive force coefficient. Finally, the angular speed of the rear tire can be obtained [29].

If the transit bus is operating at the regenerative braking process, the required braking force F_b can be determined according to the deceleration of the vehicle. Then the regenerative braking force of the rear axle F_{br} is obtained based on the following force distribution equation:

$$F_{bf} = \beta_1 F_b, \tag{2}$$

$$F_{br} = (1 - \beta_1 - \beta_2) F_b. \tag{3}$$

The model of the final drive takes into account the friction loss T_{l0}, and the inertia of rotating parts J_0 and is expressed as

$$T_m = T_w / i_0 + T_{l0} + i_0 J_0 d\omega / dt, \tag{4}$$

Parameter	Value	Unit
Vehicle mass excluding pack	9000	kg
Cargo mass	3200	kg
Dimensions	8.995 × 2.42 × 3.085	m × m × m
Rolling resistance coefficient	0.0094	—
Aerodynamic drag coefficient	0.79	—
Vehicle frontal area	7.466	m^2
Wheel radius	0.506	m
Final gear	5.833	—

Table 1.
Technical parameters of the series hybrid transit bus.

$$\omega_m = i_0\omega, \tag{5}$$

where T_w is the output torque of the final drive and T_m and ω_m are the input torque and speed of the final drive, respectively.

The electric motor model determines the requested torque T_{mr} according to the motor inertia J_m and the output torque T_m. Then the input power P_m is calculated based on a two-dimensional (2D) lookup table measured from a motor test bench.

$$T_{mr} = T_m + J_m d\omega_m/dt. \tag{6}$$

$$P_m = f(\omega_m, T_{mr}). \tag{7}$$

The mathematical model of the generator is similar to the motor.

If the detailed physical mechanism of supercapacitors is studied, an electro-chemical model or a high-order equivalent circuit model must be adopted [30]. In this study, we only consider the systematic performance of the ESS. Therefore, the RC equivalent circuit model is built using Advisor. The internal series resistance R_s and capacitance C can be obtained according to the capacitor test procedure. The relation between the current i and the voltage U_c is expressed as

$$i = \frac{dQ}{dt} = C\frac{dU_c}{dt}. \tag{8}$$

With regard to the energy conversion processes during charging or discharging, the current is obtained by

$$i = \frac{U_c - \sqrt{U_c^2 - 4R_sP_L}}{2R_s}, \tag{9}$$

where P_L is the output power of the ESS. During discharging, the energy efficiency η_{dch} is calculated as

$$\eta_{dch} = \left(1 - \frac{R_si^2}{P_L + R_si^2}\right) \times 100\%. \tag{10}$$

For charging process, the energy efficiency η_{ch} is expressed as

$$\eta_{ch} = \left(1 - \frac{R_si^2}{P_L}\right) \times 100\%. \tag{11}$$

The CNG engine model computes the requested torque T_{er} according to the engine output torque T_e and the engine speed ω_e determined by the control strategy block:

$$T_{er} = T_e + J_e d\omega_e/dt. \tag{12}$$

Subsequently, the instantaneous fuel consumption m_e is determined from a 2D map measured by an engine test bench.

$$m_e = f(\omega_e, T_{er}). \tag{13}$$

Then, the equivalent fuel consumption Q_e can be obtained according to the integral values of the fuel consumption and the driving distance using the density of diesel fuel ρ_f:

$$Q_e = \frac{\int_0^{t_f} m_e dt}{\rho_f \int_0^{t_f} v dt},\qquad(14)$$

where t_f is the final time of the driving cycle.
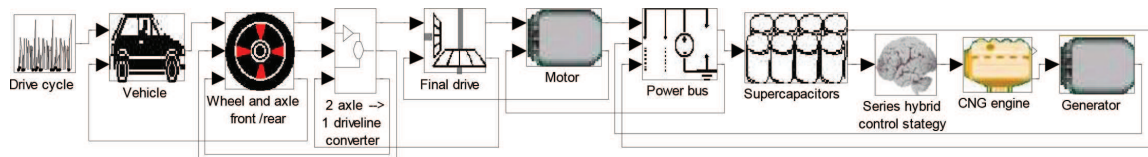
4. Control strategy design

4.1 Rule-based control strategy

To evaluate the performance of the designed series hybrid powertrain, a simulation program is developed according to the established mathematical model with MATLAB/Simulink and Advisor. Advisor is a modeling and simulation tool for hybrid electric vehicle based on MATLAB and Simulink developed by the US National Renewable Energy Laboratory [31]. The designed program is shown in **Figure 2**. Using a backward-facing method, the performance and fuel consumption of the series hybrid transit bus can be calculated. First, the driving force is determined based on the longitudinal dynamic equation. The rotating speed and driving torque of the rear axle are computed according to the tire model. Subsequently, the input torque and speed are determined for the final drive, and the input power of the motor is obtained. Then, the control strategy decides the power distribution between the ESS and the APU. As a result, both the output powers of the ESS and the APU are specified by the power bus. The supercapacitor model calculates the current and energy loss of the ESS. Moreover, the control strategy determines the operation torque and speed of the CNG engine according to the output power of the APU. Then, the fuel consumption is determined based on the performance maps of the CNG engine and the PMSG.

Rule-based control strategy takes advantage of a small computation load, which is very suitable for real-time applications. Therefore, two rule-based control strategies—the thermostatic control and the power follower control—are set up, respectively. The thermostatic control is adopted first for hybrid electric vehicles due to its simple logic. When the HEV is running, if the SOC value drops to a lower bound, the engine starts and operates at a fixed point until the SOC value reaches to an upper bound. The operation condition of the engine is set to the point with the highest effective thermal efficiency.

Large current variation in the ESS may occur for the thermostatic control strategy which results in high energy loss. Therefore, a more sophisticated power follower control is developed. According to this strategy, if the engine state is on, the output power of the APU follows the power demand of the transit bus along an optimal operation line (OOL). Hence, the output power of the APU is decreased, and the operation current of the ESS can be alleviated. The designed power follower control strategy is shown in **Figure 3**. The decision algorithm for the engine state is designed using Stateflow.

Since the power follower control needs to define an OOL, the energy efficiency characteristics of the APU must be studied first. The performance map of the CNG

Figure 2.
*The analysis program of the series hybrid powertrain.*
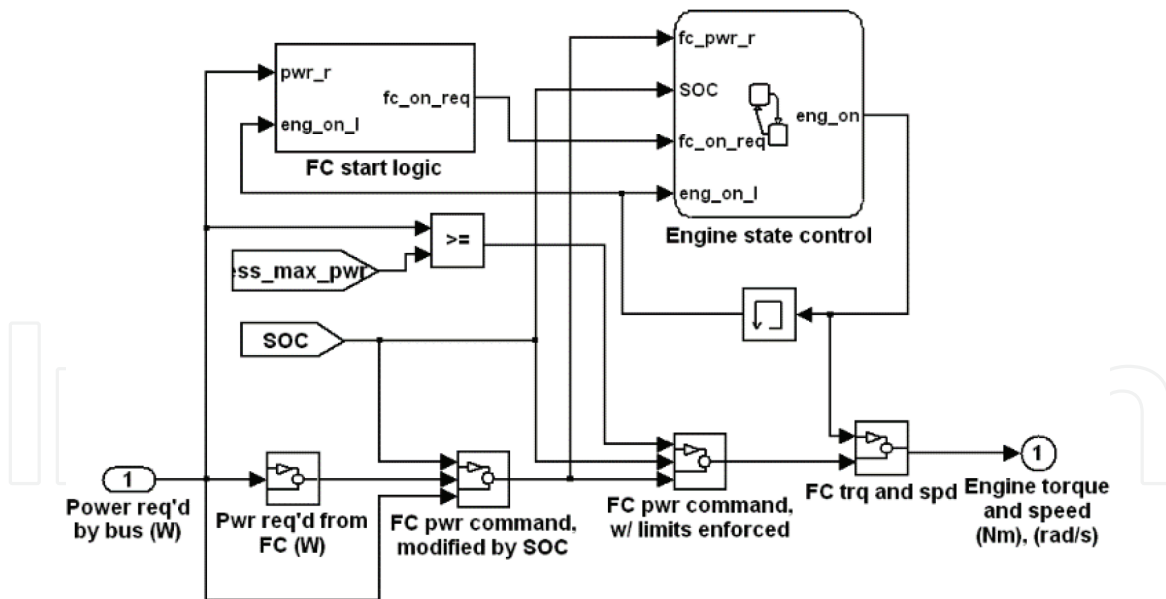
Figure 3.
The designed power follower control strategy.

engine is shown in **Figure 4a**. The blue contour denotes the engine power in kW. The black contour is the brake-specific fuel consumption (bsfc) in g/kWh. It can be seen that the minimum bsfc of the CNG engine is 196 g/kWh, which is better than that of a diesel engine. The effective thermal efficiency map of the CNG engine shown in **Figure 4b** is obtained based on the performance map of **Figure 4a**. The maximum engine efficiency achieves 36.8%, and in most of the operation regions, the effective thermal efficiency of the CNG engine is greater than 30%. The efficiency map of the PMSG is given in **Figure 4c**, where the highest energy efficiency is 94.5%. In most of the operation regions, the generator efficiency is greater than 89%. The efficiency decreases obviously if the generator speed is less than 500 r/min. According to the results of **Figure 4b** and **c**, the energy efficiency map of the APU is obtained as the product of the efficiencies of the CNG engine and the generator. The engine speed ranges from 900 to 2500 r/min, and the maximum engine torque is 650 Nm, which can be covered completely by the generator's operation domain. The results are given in **Figure 4d**. In this figure, the x-axis is the engine speed, and the y-axis is the engine torque. The blue contour represents the APU output power in kW. The black contours denote the energy efficiency of APU, which decreases with the engine torque and is greater than 30% over the regions of middle and high engine torques. The maximum efficiency is 34.06% located very close to the point with a maximum of engine torque.

Subsequently, the OOL is determined according to the efficiency map of the APU. The efficiency for each point of the OOL is the maximum at each power contour. The result is shown as the green line in **Figure 4d**. The OOL is the same with the external profile when the engine speed is greater than 1600 r/min. Meanwhile, the engine speed of the OOL remains at 900 r/min if the APU power is less than 50 kW. The OOL appears to have a U shape when the APU power is between 50 and 100 kW. Finally, the parameters of the rule-based control strategies must be optimized. The maximum energy efficiency of the APU is 34.06%. This point is denoted as point P in **Figure 8**. The corresponding engine speed and torque are 1543 r/min and 650 Nm, respectively, which are specified as the operation point of the thermostatic control strategy. The lower and upper bounds of the SOC is set to 0.58 and 0.99. The other parameters are also optimized for the power follower control strategy.
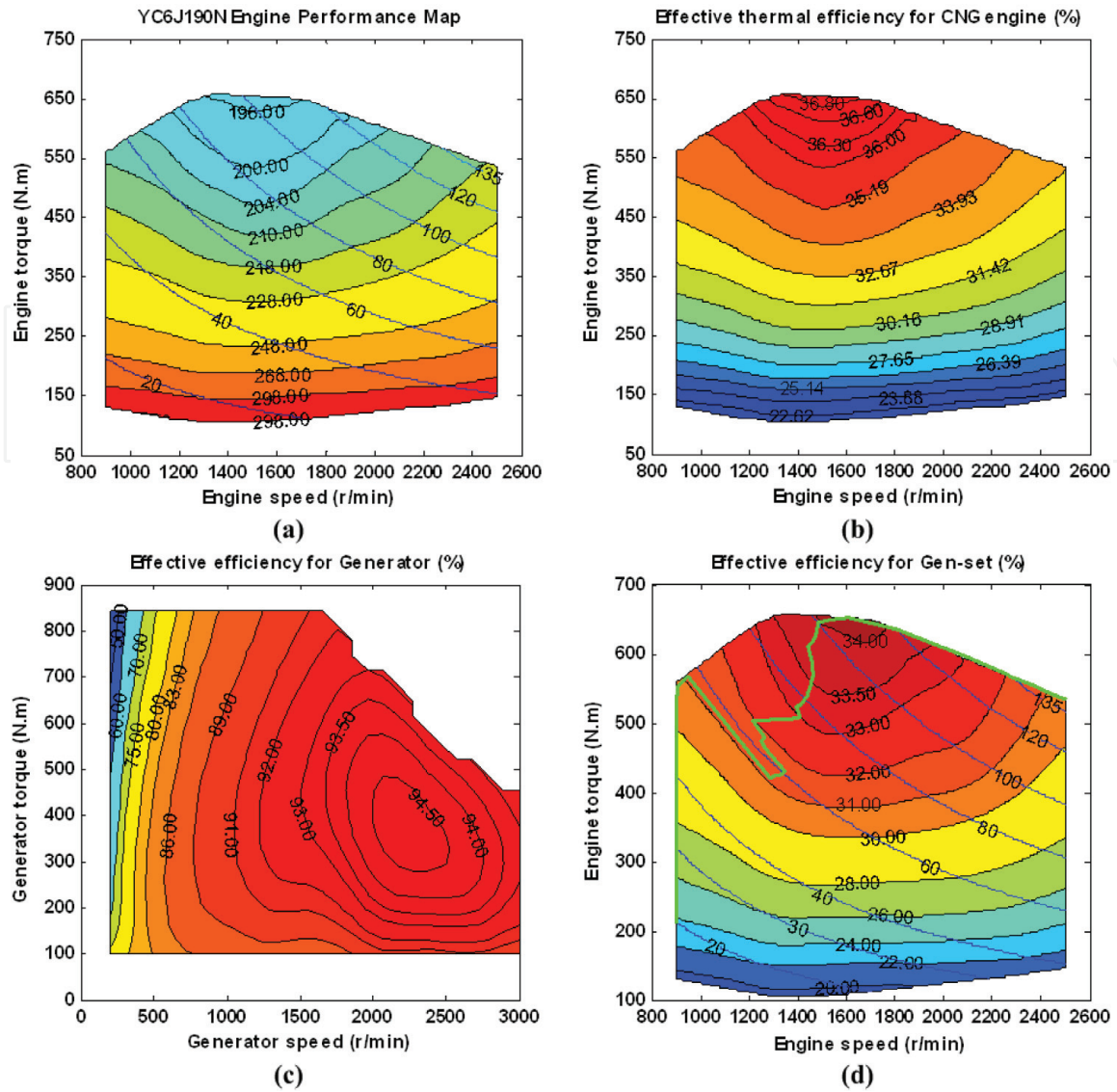
Figure 4.
Performance maps of the APU.

4.2 Optimal control using dynamic programming

In order to evaluate the maximum potential of energy savings, the theoretical minimum fuel consumption of the designed series hybrid powertrain is calculated using an optimal control algorithm based on dynamic programming. Dynamic programming is a static backward-facing optimal algorithm according to Bellman's principle of optimality. The boundary conditions of the optimal algorithm are the same with the thermostatic control.

The optimization target is the total fuel consumption based on the Chinese Transit Bus City Driving Cycle (CTBCDC). The SOC of the ESS is used as the state variable, and the output power of the APU is used as the input variable. If the output power of the APU keeps constant, the fuel consumption achieves the minimum when the CNG engine operates along the OOL. Therefore, the corresponding engine output torque and speed are determined. The target function calculates the instantaneous fuel consumption at time t and is denoted by m(x(t), u(t), t). Function F(x(t), u(t), t) is the state equation determining the SOC for the next time. The initial and final states of the SOC are set to the same values as a constraint. Moreover, the SOC and the output power of the APU must be limited within the allowable ranges all the time.

Neither the target function nor the state equation of the designed series hybrid powertrain can be expressed as an explicit equation. Therefore, the analytic solution of this optimal problem cannot be obtained. However, a numerical optimal solution can be determined by a discrete optimal model translated from the aforementioned designed program:

$$\min_{u(k)} \; J(u(k)) = \sum_{k=1}^{N-1} m_k(x(k), u(k), k), \tag{15}$$

subject to

$$\begin{cases} x(k+1) = F_k(x(k), u(k), k) \\ x(0) = s_0 \\ x(N) = s_0 \\ x(k) \in [\text{SOC}_{\min}, \text{SOC}_{\max}] \\ u(k) \in [0, P_{\text{apu, max}}] \end{cases} \tag{16}$$

Based on the established model of the series hybrid powertrain, the numerical solution of this discrete optimization problem can be determined. The solution approximates a theoretical minimum of the continuous model if the discrete computational grids for the state and input variables are fine enough. In this study, the discretization steps for the SOC and the APU output power are set to 0.005 and 1 kW, respectively. Since the total driving time of the CTBCDC is 1305 s, a time step of 1 s is used.

The optimization problem for the designed series hybrid powertrain contains the final state constraint, which can be translated to a problem without constraint via a penalty function. Sundstrom et al. have successfully applied this method to optimize the energy management problem of a parallel hybrid electric vehicle [32]. In this research, the penalty function for the state variable x_i at time stage k is defined as

$$\Phi_k(x_i(k)) = \theta(x_i(k) - S_0)^2. \tag{17}$$

Accordingly, the cost-to-go function is defined by

$$J_k(x_i(k)) = \min_{u_j(k) \in U(k)} \{m(x_i(k), u_j(k), k) + J_{k+1}[F_k(x_i(k), u_j(k), k)]\} + \Phi_k(x_i(k)). \tag{18}$$

A program is developed in MATLAB based on the designed optimal algorithm, and its working principle can be explained by **Figure 5**. The entire driving cycle is discretized along the time horizon from stage 1 to stage N shown as the yellow dashed lines. For time stage k, the state variable is discretized from SOC_{min} to SOC_{max} in a step of 0.005 and is expressed by $x_i(k)$, $i = 1, 2, ..., 79$. At each state variable $x_i(k)$, the value of the cost-to-go function is denoted by $J_i(k)$, and the corresponding penalty function is $\Phi_i(k)$. The input variable is discretized from 0 to $P_{apu,max}$ in a step of 1 kW and is denoted by $u_j(k)$, $j = 1, 2, ..., 136$. The fuel consumption from stage k to stage $k + 1$ at the state $x_i(k)$ is denoted by the function $m_i(k)$. The initial and final states are constrained to the two red points S_0 shown in **Figure 5**.

The algorithm first calculates the penalty function J_N at the last stage for the state vector x_i:

$$J_N(x_i) = \theta(x_i - S_0)^2. \tag{19}$$

Then taking into account each state variable of stage $N - 1$, a state vector at the next time stage is computed corresponding to the input variable vector based on the state equation. This process is described by a group of lines from one state point of stage $N - 1$ to different positions of stage N. Because the calculated state vector for stage N may not locate exactly at the computational grid points, a linear interpolation is used to determine the values of the corresponding cost-to-go function. Meanwhile, the fuel consumption function for each state variable is calculated. As a result, the values of cost-to-go function at time stage $N - 1$ is obtained according to Eq. (18). The optimal path for each state variable is represented by a blue line in **Figure 5**. The above recurrence calculation process is repeated along the time horizon one by one until to the first time stage. Finally, an optimal map of the cost-to-go function for all the time stages and the state variables is obtained.

In order to determine the optimal policy, a forward calculation process is performed based on the optimal map. The following equation is used to compute the minimum fuel consumption from the initial state S_0 to the same final state, and the corresponding input variable is recorded:

$$M(k) = \min_{u_j(k) \in U(k)} \left\{ m\left(x_{op}(k), u_j(k), k\right) + J_{k+1}\left[F_k\left(x_{op}(k), u_j(k), k\right)\right] \right\}. \tag{20}$$

where $x_{op}(k)$ is the optimal state variable at stage k. The optimal state value for the next time stage is determined by

$$x_{op}(k+1) = x_{op}(k) + \frac{(P_m(k) - u(k))C(k)}{U_0^2 x_{op}(k)}, \tag{21}$$

where U_0 is the rated voltage of the ESS. Repeating the calculation process until the last time stage, an optimal policy is obtained shown as the green line in **Figure 5**. The algorithm uses a weighting factor θ for the penalty function whose value specifies the importance of the SOC deviation relative to the fuel consumption. In order to make the final state of the optimal path converge to S_0, various values of θ are tried. Finally, a value of 120 is specified, and the relative error of the SOC at the last state is 0.44%.
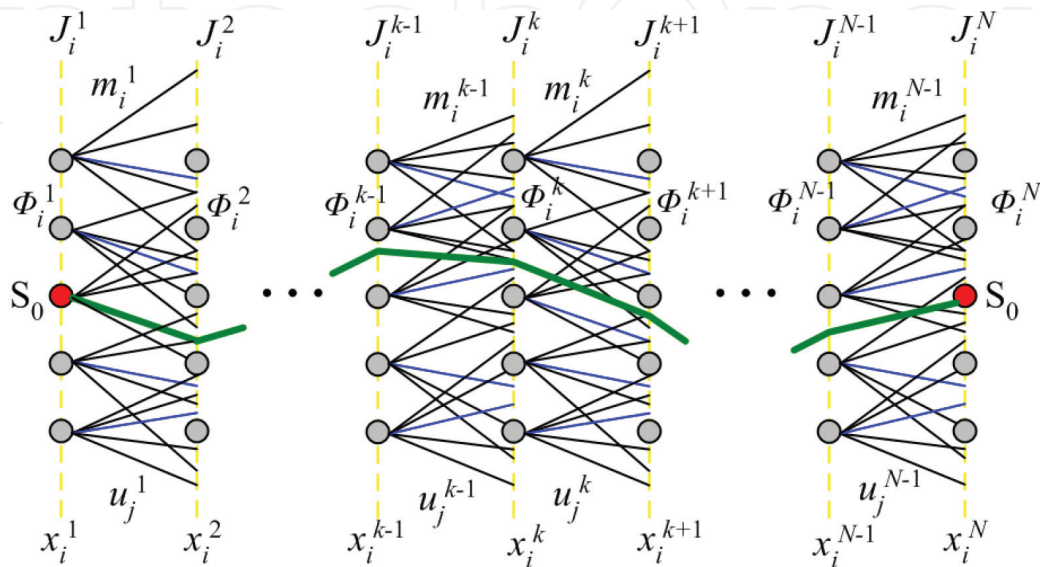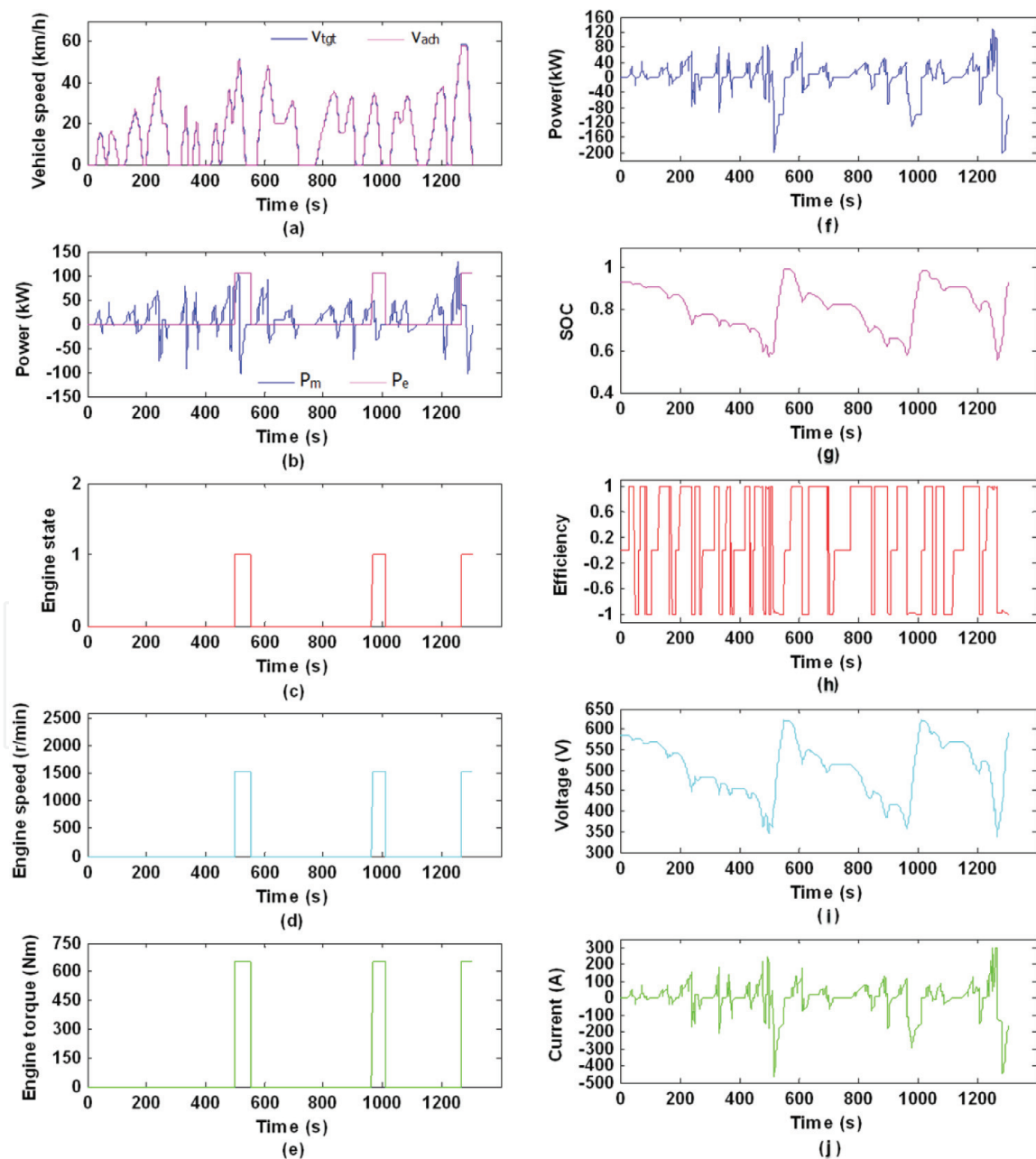

Figure 5.
Principle of the optimal algorithm based on dynamic programming.

5. Result analysis

5.1 Comparison of rule-based control strategies

The system performance and fuel economy of the series hybrid transit bus are evaluated using the CTBCDC driving cycle. The performances of the thermostatic control and the power follower control are compared. The results of the thermostatic control strategy are given in **Figure 6**. **Figure 7** shows the results of the power follower strategy.

The target vehicle speed and the achievable vehicle speed are given in **Figures 6a** and **7a**, which are denoted by the blue and magenta lines, respectively. The achievable vehicle speeds for both of the rule-based strategies can trace the target one perfectly. Therefore, both can satisfy the requirements of drivability. **Figure 6b** shows the input power of the PMSM as the blue lines and the output power of the CNG engine by the red lines. **Figure 7b** shows the results of the power

Figure 6.
*System performance of the thermostatic control strategy.*
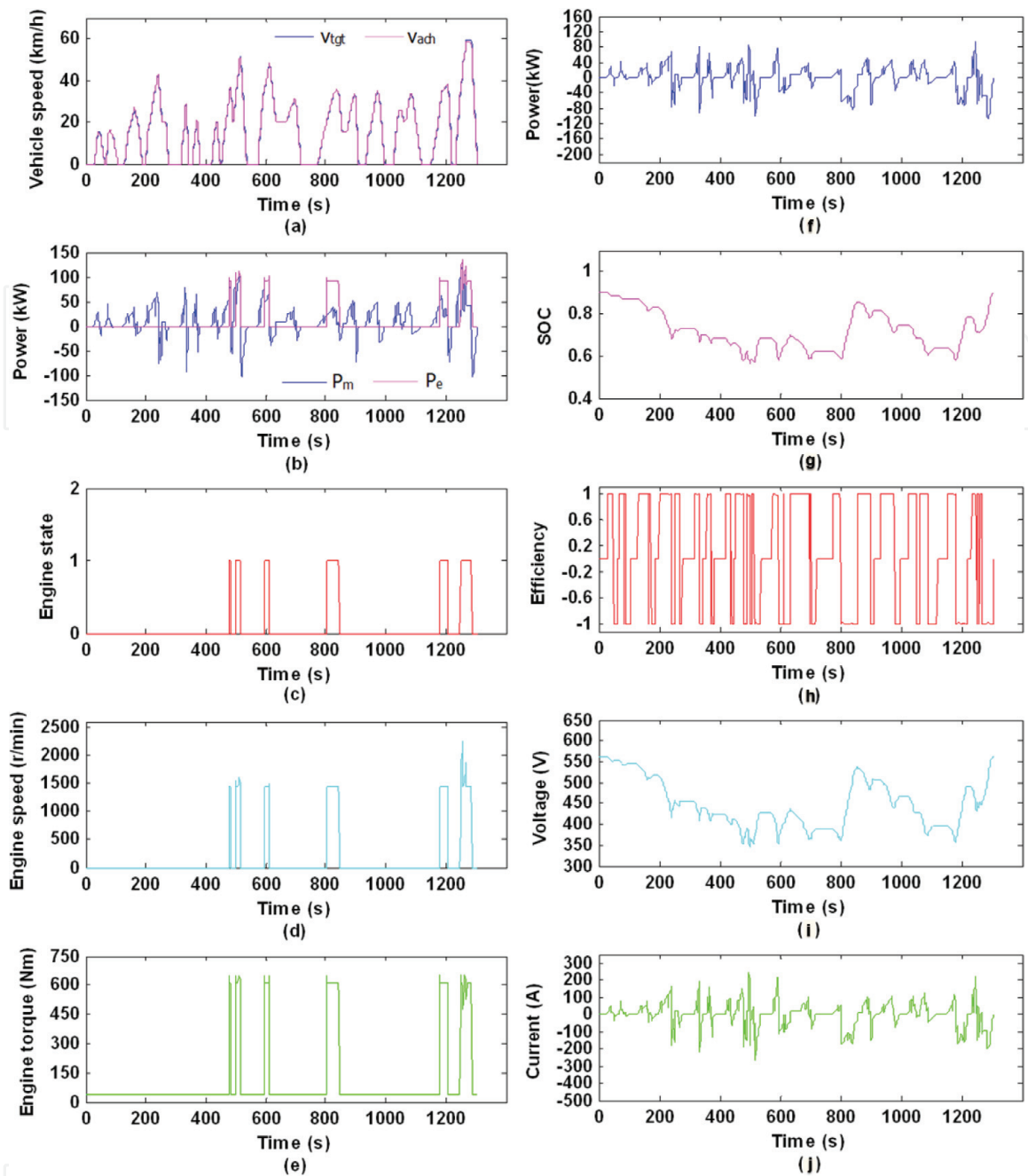
Figure 7.
System performance of the power follower control strategy.

follower strategy. The engine operation time of the thermostatic control is less than that of the power follower strategy, which is 141 s for the thermostatic control while 151 s for the power follower control. The engine power keeps constant for the thermostatic control. However, the engine power of the power follower control varies along the OOL within a small range. The results of the engine state for these two control strategies are shown in **Figures 6c** and **7c,** where the engine state ON is represented by 1, and the engine state OFF is denoted by 0. The engine demonstrates a regular alternative start and stop for the thermostatic control, whereas the engine starts more frequently for the power follower control, which will worsen the engine emissions. The engine speed and torque are shown in **Figure 6d** and **e** for the thermostatic control. Compared to the results of the power follower control given in **Figure 7d** and **e,** the engine can operate more stably for the thermostatic control, which will be beneficial for the engine working life.

The output power of the ESS for the thermostatic control is shown in **Figure 6f**, where the positive values mean discharging and the negative values denote charging (this expression is used for the following figures). **Figure 7f** shows the results of the power follower control. Both output powers vary all the time except for the stopping conditions. Furthermore, the variation magnitude of the thermostatic control is obviously greater than that of the power follower control. The maximum discharging power for the thermostatic control is 126.8 kW, while this value reduces to 95.68 kW for the power follower control. By contrast, the maximum charging power of the ESS for the thermostatic control is 202.8 kW, while this value reduces significantly to 106.6 kW for the power follower control. The profiles of the SOC are given in **Figures 6g** and **7g**, respectively. In terms of the thermostatic control, the SOC shows an alternative variation process that first decreases slowly then increases rapidly. However, the SOC of the power follower control shows a relative slow augmentation process, which is in favor of the life span of the ESS.

The energy efficiencies of the ESS are obtained according to Eqs. (10) and (11). The results are given in **Figures 6h** and **7h**. The average discharging and charging efficiencies of the power follower control are 99.1 and 98.5%. As a contrast, these two values are 99.1 and 98.4% for the thermostatic control. The results indicate that the energy efficiency of the power follower control is slightly higher than the thermostatic control. The energy efficiency of supercapacitor will decrease obviously if the operation temperature is too high. Therefore, a temperature control system for the ESS is required in practice. The voltage profiles are given in **Figures 6i** and **7i**. Both of them operate within the constraint range. The average voltage for the power follower control is 450 V, while the average voltage is 505 V for the thermostatic control. Enhancement of the operation voltage is helpful to improve the energy efficiency of the electric motor. Because the SOC value has a linear relation with the operation voltage, the variation tendency of the SOC is consistent with that of the voltage. The current profiles are given in **Figures 6j** and **7j**. The maximum discharging and charging currents for the power follower control are 247 and 269 A. However, these two values are increased significantly to 300 and 471 A for the thermostatic control. Although supercapacitors can work with a high power rate, a lower current will be in favor of their life span. Therefore, it seems that the power follower control strategy is better than the thermostatic control.

Table 2 gives the equivalent fuel consumptions of these strategies. The equivalent fuel consumption is 17.32 L/100 km for the power follower strategy, while it equals 17.51 L/100 km for the thermostatic control strategy. In contrast to a conventional vehicle powered solely by the same CNG engine, the fuel consumptions of the two rule-based strategies are decreased by 52%. **Figure 8** is used to explain the reason from a viewpoint of energy efficiency. The OOL is displayed as the green line. Point P is the operation point of the thermostatic control whose energy efficiency is 34.06%. Because most of the APU output power of the thermostatic control first charges to the ESS and then outputs to the power line, the overall energy efficiency of the series hybrid powertrain decreases slightly to 33.2%, which is denoted by a blue contour L in **Figure 8**. The operation points of the power follower control are described by the cyan points. Most of the APU output power is delivered directly to the power line for the power follower strategy. The energy efficiencies for the thermostatic control approximate the line L, while the energy efficiencies of the power follower control remain at the cyan points. Therefore, the fuel economy of the power follower control is a little higher than that of the thermostatic control.
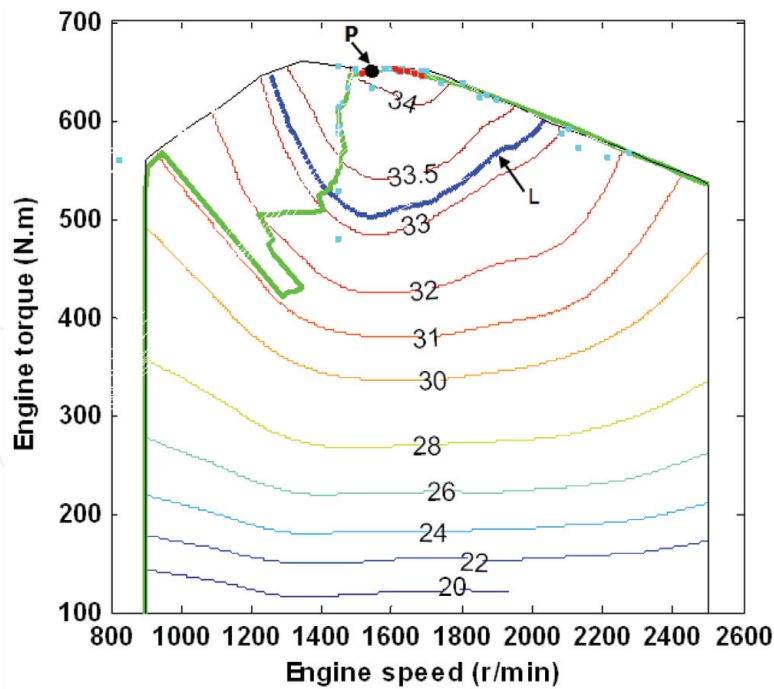
Figure 8.
*Comparison of energy efficiencies of different control strategies.*

Powertrain	Fuel consumption (L/100 km)	Energy reduction (%)[a]
Conventional bus using a CNG engine	36.60	
Hybrid bus using the thermostatic control	17.51	52.2
Hybrid bus using the power follower control	17.32	52.7
Hybrid bus using optimal control	15.72	57.1

[a]*Relative to the conventional bus with a CNG engine.*

Table 2.
Results of fuel consumption.

5.2 Results of optimal control

The optimal performance of the series hybrid powertrain is shown in **Figure 9**. **Figure 9a** is the velocity profile of the CTBCDC cycle. The corresponding input power required by the PMSM is shown in **Figure 9b**, where the positive values are used for the driving mode and the negative values are used for the regenerative braking mode. These two profiles are used as input parameters for the optimal algorithm. The optimal results of the output power of the APU are given in **Figure 9c**, which demonstrates a series of short impulse when the transit bus undergoes an acceleration process. Furthermore, the number of the impulse increases as the power demand of the motor rises. The APU stops if the power demand of the motor is negative. The corresponding engine output torque and speed are shown in **Figure 9d** and **e**, respectively. The optimal engine speed and torque remain around 1500 r/min and 600 Nm. The reason for such an optimal trajectory can be explained as follows. The operation points of the CNG engine for the optimal control are described by the red points in **Figure 8**. These red points are very close to the point P where the energy efficiency is the highest. Therefore, an overall minimum of the fuel consumption is realized. On the other hand, the
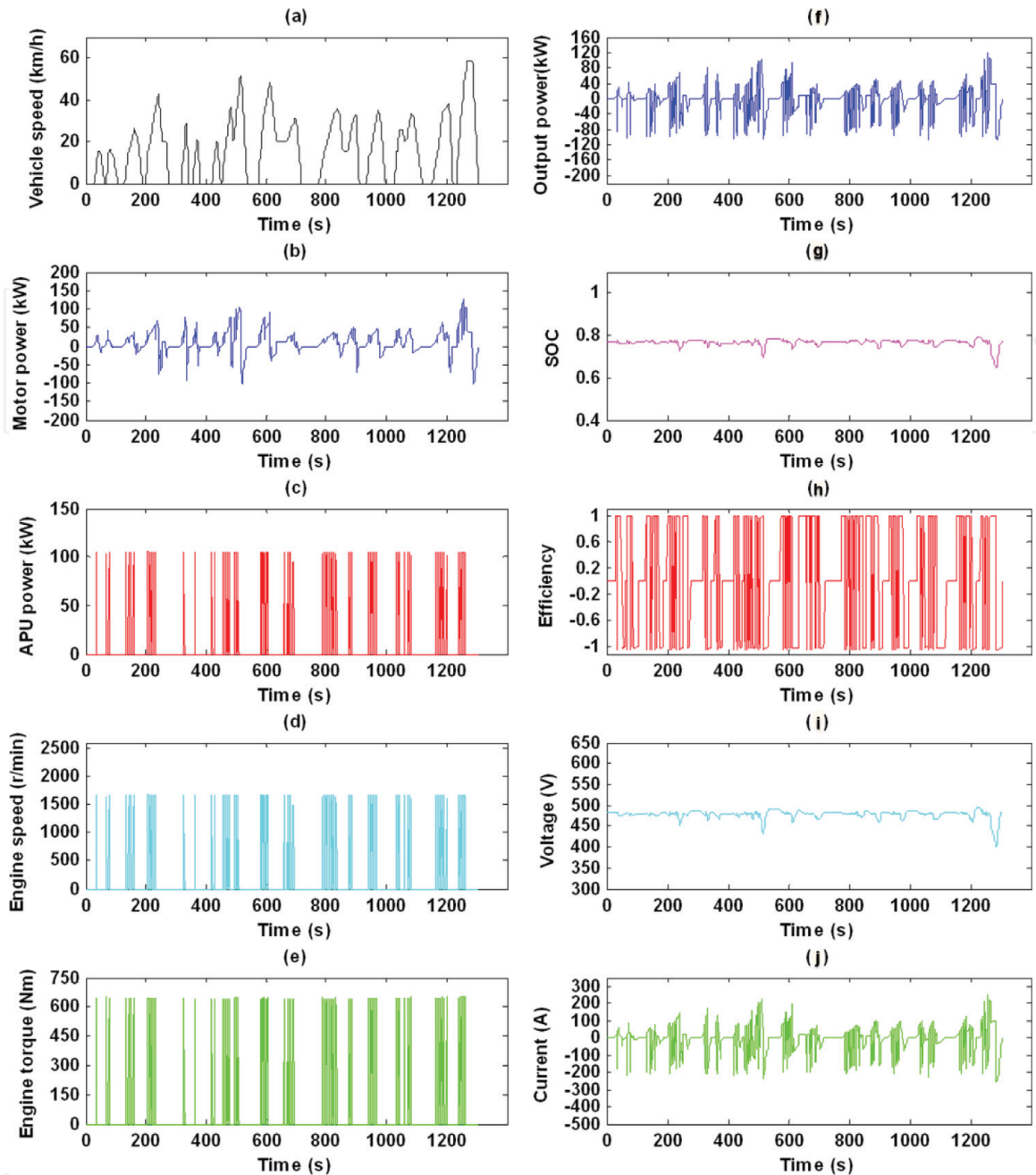
Figure 9.
System performance of the optimal control by dynamic programming.

internal series resistance of the ESS consumes part of the energy during the charging or discharging process, especially for large current conditions. To avoid too much energy loss of the ESS, the optimal policy will try to use the APU power to satisfy the power demand of the PMSM exactly. In other words, the optimal policy is obtained if the APU operates at the maximum energy efficiency point and the amount of the output power equals to the power demand of the PMSM, leading to the energy supply in the form of a series of impulse.

The output power of the supercapacitors is given in **Figure 9f**. Generally, the variation tendency of the output power is similar to that of the power follower control shown in **Figure 7f**. However, a series of impulses occur under the driving modes due to the same reason for the output power of the APU. The SOC profile is given in **Figure 9g**. The optimal SOC remains within a small interval around the initial valleys. Only two valleys occur at the high-velocity condition with rapid braking. The energy loss of the ESS is decreased if the current of the ESS is limited

within a small range. Thus, the fuel consumption can be reduced. The calculated energy efficiencies of the ESS are shown in **Figure 9h**. The average energy efficiency is very close to the results of the rule-based strategies. The output voltage and current are given in **Figures 9i** and **j**, respectively. The output voltage is proportional to the SOC. The optimal current demonstrates a similar tendency as that of the power follower control. However, more spikes occur at the driving conditions.

The optimal equivalent fuel consumption is 15.72 L/100 km listed in **Table 2**. Compared to the conventional transit bus, the optimal fuel consumption of the hybrid bus can be decreased by 57% if the quantity of fuel consumed during the starting processes is ignored. In practice, the fuel consumption including starting process will be increased slightly. Taking the optimal result as a reference, the fuel consumptions of the rule-based control strategies are increased by approximate 1.7 L/100 km.

6. Conclusions

In this chapter, the energy efficiency of a series hybrid transit bus powered by a CNG engine and supercapacitors was evaluated. A mathematical model was established, and three different control strategies were designed. The performance characteristics of two rule-based control strategies were compared to the result of the optimal control using dynamic programming. Based on our analysis, the following can be concluded:

1. The performance of the designed series hybrid transit bus powered by a CNG engine and supercapacitors can fulfill the requirements of the vehicle. Because supercapacitors take advantage of low energy loss and can recover the vehicle's kinetic energy efficiently during regenerative braking, the fuel consumption of the designed series hybrid powertrain is decreased significantly by approximately 52% compared to a conventional transit bus under the CTBCDC driving cycle. The results indicate that supercapacitors are a good solution for the ESS of the hybrid transit bus.

2. The energy efficiency of the designed series hybrid transit bus using the power follower control strategy is slightly greater than that of the thermostatic control strategy because the operation current of the ESS remains at a low level. The thermostatic control has a relatively simple logic and less starting times compared with the power follower control. In practice, the most suitable control strategy should be selected according to the requirements of system performance including efficiency, cost, size, reliability, emissions, and so on.

3. The maximum energy efficiency of the designed series hybrid powertrain is estimated using an optimal algorithm based on dynamic programming. The optimal fuel consumption can be decreased by 57% compared to the results of the conventional transit bus. Although the fuel consumption from the rule-based control strategies is slightly higher than that of the optimal control, taking into account the operation requirements of the engine, the rule-based control strategies are more practical for real-time application. However, the result of the optimal control provides some useful insights for real-time control strategy design.

Acronyms

APU	auxiliary power unit
bsfc	brake-specific fuel consumption
CNG	compressed natural gas
CTBCDC	Chinese Transit Bus City Driving Cycle
EDLC	electrochemical double-layer capacitor
ESS	energy storage system
EV	electric vehicle
HESS	hybrid energy storage system
HEV	hybrid electric vehicle
OOL	optimal operation line
PHEV	plug-in hybrid electric vehicle
PMSG	permanent magnetic synchronous generator
PMSM	permanent magnetic synchronous motor
SOC	state of charge

Conflict of interest

The authors declare no conflict of interest.

Author details

Enhua Wang[1*], Minggao Ouyang[2], Fujun Zhang[1] and Changlu Zhao[1]

1 School of Mechanical Engineering, Beijing Institute of Technology, Beijing, China

2 State Key Laboratory of Automotive Safety and Energy, Tsinghua University, Beijing, China

*Address all correspondence to: enhua.wang@yahoo.com

IntechOpen

References

[1] Silva C. At what extent the benefits of introducing alternative light-duty vehicles offset those of increasing the buses average occupancy? Energy Conversion and Management. 2013;**70**: 211-219

[2] Bayindir KC, Gozukucuk MA, Teke A. A comprehensive overview of hybrid electric vehicle: Powertrain configurations, powertrain control techniques and electronic control units. Energy Conversion and Management. 2011;**52**:1305-1313

[3] Sharma P, Bhatti TS. A review on electrochemical double-layer capacitors. Energy Conversion and Management. 2010;**51**:2901-2912

[4] Mellincovsky M, Kuperman A, Lerman C, Aharon I, Reichbach N, Geula G, et al. Performance assessment of a power loaded supercapacitor based on manufacturer data. Energy Conversion and Management. 2013;**76**: 137-144

[5] Farkas A, Bonert R. Ultracapacitors as sole energy storage device in hybrid electric cars? In: Proceedings IEEE Power Electronics in Transportation, 1994 Oct 20–21, Dearborn, MI, IEEE. 1994. pp. 97-101

[6] Burke A. Ultracapacitor technologies and application in hybrid and electric vehicles. International Journal of Energy Research. 2010;**34**:133-151

[7] Vinot E, Trigui R. Optimal energy management of HEVs with hybrid storage system. Energy Conversion and Management. 2013;**76**:437-452

[8] Yassine M, Fabris D. Performance of commercially available supercapacitors. Energies. 2017;**10**:1340

[9] Wang E, Guo D, Yang F. System design and energetic characterization of a four-wheel-driven series-parallel hybrid electric powertrain for heavy-duty applications. Energy Conversion and Management. 2015;**106**: 1264-1275

[10] Barbosa FC. Ultracapacitor Transit Bus—Urban Electric Mobility into an Opportunity Charging Concept. SAE Paper 2016-36-0176

[11] Wang E, Yang F, Ouyang M. A hybrid energy storage system for a coaxial power-split hybrid powertrain. In: Donateo T, editor. Hybrid Electric Vehicle. Croatia: InTech; 2017. pp. 83-104

[12] Veneri O, Capasso C, Patalano S. Experimental investigation into the effectiveness of a super-capacitor based hybrid energy storage system for urban commercial vehicles. Applied Energy. 2017. DOI: 10.1016/j.apenergy.2017. 08.086

[13] Geetha A, Subramani C. A comprehensive review on energy management strategies of hybrid energy storage system for electric vehicles. International Journal of Energy Research. 2017;**41**:1817-1834

[14] Min H, Lai C, Yu Y, Zhu T, Zhang C. Comparison study of two semi-active hybrid energy storage systems for hybrid electric vehicle applications and their experimental validation. Energies. 2017;**10**:279

[15] Song Z, Zhang X, Li J, Hofmann H, Ouyang M, Du J. Component sizing optimization of plug-in hybrid electric vehicles with the hybrid energy storage system. Energy. 2018;**144**:393-403

[16] Kouchachvili L, Yaici W, Entchev E. Hybrid battery/supercapacitor energy storage system for the electric vehicles. Journal of Power Sources. 2018;**374**: 237-248

[17] Salmasi FR. Control strategies for hybrid electric vehicles: Evolution, classification, comparison, and future trends. IEEE Transactions on Vehicular Technology. 2007;**56**:2393-2404

[18] Chau KT, Wong YS. Overview of power management in hybrid electric vehicles. Energy Conversion and Management. 2002;**43**:1953-1968

[19] Sorrentino M, Rizzo G, Arsie I. Analysis of a rule-based control strategy for on-board energy management of series hybrid vehicles. Control Engineering Practice. 2011;**19**:1433-1441

[20] Li SG, Sharkh SM, Walsh FC, Zhang CN. Energy and battery management of a plug-in series hybrid electric vehicle using fuzzy logic. IEEE Transactions on Vehicular Technology. 2011;**60**: 3571-3585

[21] Jalil N, Kheir NA, Salman M. A rule-based energy management strategy for a series hybrid vehicle. In: Proceedings of the 1997 American Control Conference, 1997 Jun 4–6, Albuquerque, NM, Vol. 1, IEEE. 1997. pp. 689-693

[22] Hung YH, Wu CH. An integrated optimization approach for a hybrid energy system in electric vehicles. Applied Energy. 2012;**98**:479-490

[23] Xiong W, Zhang Y, Yin C. Optimal energy management for a series–parallel hybrid electric bus. Energy Conversion and Management. 2009;**50**:1730-1738

[24] Perez LV, Bossio GR, Moitre D, Garcia GO. Optimization of power management in a hybrid electric vehicle using dynamic programming. Mathematics and Computers in Simulation. 2006;**73**:244-254

[25] Anatone M, Cipollone R, Donati A, Sciarretta A. Control-oriented modeling and fuel optimal control of a series hybrid bus. In: SAE Paper 2005–01-1163. 2005

[26] Konev A, Lezhnev L, Kolmanovsky I. Control strategy optimization for a series hybrid vehicle. In: SAE Paper 2006-01-0663. 2006

[27] Nguyen A, Lauber J, Dambrine M. Optimal control based algorithms for energy management of automotive power systems with battery/supercapacitor storage devices. Energy Conversion and Management. 2014;**87**: 410-420

[28] Moreno J, Ortuzar ME, Dixon JW. Energy-management system for a hybrid electric vehicle, using ultracapacitors and neural networks. IEEE Transactions on Industrial Electronics. 2006;**53**:614-623

[29] Ouyang M, Zhang W, Wang E, Yang F, Li J, Li Z, et al. Performance analysis of a novel coaxial power-split hybrid powertrain using a CNG engine and supercapacitors. Applied Energy. 2015;**157**:595-606

[30] Wu CH, Hung YH, Hong CW. On-line supercapacitor dynamic models for energy conversion and management. Energy Conversion and Management. 2012;**53**:337-345

[31] Advisor documentation. US: National Renewable Energy Laboratory; 2013

[32] Sundstrom O, Ambuhl D, Guzzella L. On implementation of dynamic programming for optimal control problems with final state constraints. Oil & Gas Science and Technology. 2010; **65**(1):91-102